

1 **TITLE**

2 Exploring the impact of digestive physicochemical parameters of adults and infants on the
3 pathophysiology of *Cryptosporidium parvum* using the dynamic TIM-1 gastrointestinal model

4 **AUTHORS**

5 Julie Tottey¹, Lucie Etienne-Mesmin², Sandrine Chalançon², Alix Sausset¹, Sylvain Denis², Carine
6 Mazal², Christelle Blavignac³, Guillaume Sallé¹, Fabrice Laurent¹, Stéphanie Blanquet-Diot², Sonia
7 Lacroix-Lamandé¹

8 ¹UMR 1282 ISP, Infectiologie et Santé Publique, INRAE, Université de Tours, Nouzilly, France;

9 ²UMR 454 MEDIS, Microbiologie Environnement Digestif et Santé, Université Clermont Auvergne,

10 INRAE, Clermont-Ferrand, France; ³Centre Imagerie Cellulaire Santé, Université Clermont Auvergne,

11 Clermont-Ferrand, France.

12 Corresponding author: Julie Tottey

13 **ABSTRACT**

14 **Background**

15 Human cryptosporidiosis is distributed worldwide, and it is recognised as a leading cause of acute
16 diarrhoea and death in infants in low- and middle-income countries. Besides immune status, the higher
17 incidence and severity of this gastrointestinal disease in young children could also be attributed to the
18 digestive environment. For instance, human gastrointestinal physiology undergoes significant changes
19 with age, however the role this variability plays in *Cryptosporidium parvum* pathogenesis is not
20 known. In this study, we analysed for the first time the impact of digestive physicochemical

21 parameters on *C. parvum* infection in a human and age-dependent context using a dynamic *in vitro*
22 gastrointestinal model.

23 **Results**

24 Our results showed that the parasite excystation, releasing sporozoites from oocysts, occurs in the
25 duodenum compartment after one hour of digestion in both child (from 6 months to 2 years) and adult
26 experimental conditions. In the child small intestine, slightly less sporozoites were released from
27 excystation compared to adult, however they exhibited a higher luciferase activity, suggesting a better
28 physiological state. Sporozoites collected from the child jejunum compartment also showed a higher
29 ability to invade human intestinal epithelial cells compared to the adult condition. Global analysis of
30 the parasite transcriptome through RNA-sequencing demonstrated a more pronounced modulation in
31 ileal effluents compared to gastric ones, albeit showing less susceptibility to age-related digestive
32 condition. Further analysis of gene expression and enriched pathways showed that oocysts are highly
33 active in protein synthesis in the stomach compartment, whereas sporozoites released in the ileum
34 showed downregulation of glycolysis as well as strong modulation of genes potentially related to
35 gliding motility and secreted effectors.

36 **Conclusions**

37 Digestion in a sophisticated *in vitro* gastrointestinal model revealed that invasive sporozoite stages are
38 released in the small intestine, and are highly abundant and active in the ileum compartment,
39 supporting reported *C. parvum* tissue tropism. Our comparative analysis suggests that
40 physicochemical parameters encountered in the child digestive environment can influence the amount,
41 physiological state and possibly invasiveness of sporozoites released in the small intestine, thus
42 potentially contributing to the higher susceptibility of young individuals to cryptosporidiosis.

43 **KEYWORDS**

44 *Cryptosporidium*; Apicomplexa; *in vitro* digestive model; physicochemical parameters; child and adult
45 digestion

46 **BACKGROUND**

47 The zoonotic disease cryptosporidiosis caused by the protozoan Apicomplexa parasite
48 *Cryptosporidium* is endemic in many low-income countries and potentially epidemic in high-income
49 countries. This enteric disease leads to watery diarrhoea that can be life-threatening in individuals with
50 an immature or a compromised immune system. Results from cohort studies have consistently shown
51 that young age is associated with a higher risk of *Cryptosporidium* infection (1). Accordingly,
52 *Cryptosporidium* infection is particularly associated with prolonged (7–14 days) or even persistent (\geq
53 14 days) diarrhoea during childhood, and can also lead to malnutrition and growth deficiency (1).
54 Cryptosporidiosis is considered as one of the most common causes of infectious moderate-to-severe
55 diarrhoea in children under the age of two (2,3) and an important contributor to early childhood
56 mortality in low-resource settings (4), thus constituting a serious public health concern. In 2016, acute
57 infections due to *Cryptosporidium* caused more than 48000 deaths in children under 5 years and more
58 than 4.2 million disability-adjusted life-years lost (5).

59 *Cryptosporidium parvum* is one of the two most relevant *Cryptosporidium* species to humans and is
60 transmitted primarily by the fecal–oral route either by direct contact with an infected human or animal
61 or indirectly via food or water contaminated by oocysts (6). Once ingested, *C. parvum* oocysts excyst
62 in the gastrointestinal tract, releasing infective and motile sporozoites that invade intestinal epithelial
63 cells. The parasite life cycle then progresses through three rounds of asexual replication (7) before
64 shifting to sexual reproduction and then to the production of a high number of infectious oocysts that
65 ensure either auto-infection of the same host by infecting nearby intestinal cells or transmission in the
66 environment after release in the faeces.

67 The higher incidence and severity of cryptosporidiosis reported in children under the age of two can be
68 first attributed to their immature immune status, making them as susceptible to the infection by the
69 parasite as immunocompromised adults (8). Nevertheless, other factors, such as those associated with
70 the digestive environment (*i.e.*, immaturity of digestive processes, intestinal epithelium and resident
71 microbiota) where *C. parvum* infection takes place, could also contribute to the age-dependent nature
72 of symptomatic cryptosporidiosis. Consequently, there is a crucial need to investigate *C. parvum*
73 pathogenesis considering the gastrointestinal physiology that varies greatly with age (9), especially in
74 light of the differences in digestive physicochemical parameters encountered in children, compared to
75 adults.

76 Due to obvious ethical and technical reasons, it remains very difficult to evaluate the pathophysiology
77 of food- or water-borne pathogens in the human gastrointestinal tract, especially in pediatric
78 populations. *In vitro* gastrointestinal models represent an appropriate alternative to *in vivo* assays to
79 study the impact of digestive physicochemical parameters alone (*i.e.*, independently of any other
80 influencing factors from the host) in a nutritional, pharmaceutical, toxicological or microbiological
81 context. Among the available gastrointestinal systems, the computer-controlled TNO (Toegepast
82 Natuurwetenschappelijk Onderzoek) gastroIntestinal Model-1 (TIM-1), which combines multi-
83 compartmentalisation and dynamism, is one of the most complete *in vitro* simulators of the human
84 upper gastrointestinal tract (10). By reproducing physiologically relevant conditions, the TIM-1
85 system allows the closest simulation of *in vivo* dynamic events occurring within the human stomach
86 and three compartments of the small intestine. As a result, it has been successfully used for a diversity
87 of applications in the past, for instance in an array of pathogen-related microbiological studies (10–
88 16). As an example, the TIM-1 model has been used to demonstrate that the variability in human
89 digestive physicochemical parameters that occurs between child and adult populations could play a
90 role in *E. coli* O157:H7 pathogenesis, which is considerably more severe in children than in adults
91 (12).

92 Within this framework, we designed an original approach to question for the first time the impact of
93 digestive physicochemical parameters on *C. parvum* infection, in a human and age-dependent context.

94 The aim of the present study was to use the sophisticated TIM-1 model for a comparative analysis of
95 *C. parvum* infection under the digestive conditions encountered in young children (from 6 months to 2
96 years) or in adults following the simulated digestion of a glass of contaminated water. Various parasite
97 parameters, from the parasite excystation kinetics and global gene expression, to the sporozoite
98 physiological state and infectivity, were monitored throughout the simulated human digestions.

99 **METHODS**

100 **Cells and parasites**

101 Human ileocecal adenocarcinoma cells (HCT-8) were purchased from the American Type Culture
102 Collection, cultured in RPMI 1640 with phenol red supplemented with 2 mM GlutaMAX™, 10%
103 (v/v) heat-inactivated fetal bovine serum (FBS), 1 mM sodium pyruvate, 50 U/ml penicillin, and 50
104 µg/ml streptomycin and maintained at 37°C in a humidified atmosphere under 5% CO₂. The *C.*
105 *parvum* INRAE Nluc strain was generated by transgenesis to produce Nluc-expressing parasites, and
106 purified as described in Swale *et al.*, 2019 (17).

107 ***In vitro* digestions in the TIM-1 gastrointestinal model**

108 The TIM-1 model (TNO, Zeist, The Netherlands) consists of four successive compartments simulating
109 the human stomach and the three segments of the small intestine (duodenum, jejunum, and ileum)
110 (Figure 1). The main parameters of digestion, such as body temperature, pH, peristaltic mixing and
111 transport, gastric, biliary, and pancreatic secretions and passive absorption of small molecules and
112 water, are reproduced as accurately as possible, as already described (16). The TIM-1 system was
113 programmed to reproduce, based on *in vivo* data, the physicochemical digestive conditions observed in
114 a healthy adult or a young child (from 6 months to 2 years) when a glass of water is ingested as
115 previously described (12). The TIM-1 system was inoculated with a parasite suspension consisting of
116 200 mL of mineral water (Volvic®, Danone, France) experimentally contaminated with 1×10^8
117 oocysts of the *C. parvum* INRAE Nluc strain. Two sets of experiments were performed: gastric

118 digestions where the stomach compartment was solely used (total duration of 60 min) and
119 gastrointestinal digestions using the entire TIM-1 model (total duration of 300 min). Digestions were
120 run in triplicate.

121 **TIM-1 sampling**

122 Samples were taken in the initial parasite suspension (t=0) and regularly collected during *in vitro*
123 digestions from each digestive compartment (stomach, duodenum, jejunum, and ileum) to evaluate
124 parasite excystation kinetics, sporozoite luciferase activity and host cell invasion (Figure 1). Gastric
125 and ileal effluents were also collected on ice and pooled on 0-20, 20-45, and 45-60 min for gastric
126 digestions and hour-by-hour during 5 h for gastrointestinal digestions. Gastric and ileal effluents
127 collected during 0-20 min and 120-180 min, respectively, were used for RNA extraction.

128 **Parasite excystation kinetics**

129 The parasite excystation success was monitored in three independent experiments by flow cytometry
130 from samples collected regularly from each digestive compartment during *in vitro* digestions in the
131 TIM-1 system. Prior to each TIM-1 digestion assay, flow cytometry controls and gating strategy on
132 forward-angle light scatter/side-angle light scatter were performed based on analysis of intact (non-
133 excysted) oocysts, and non-filtered or 5 µm-filtered (Sartorius AG, Göttingen, Germany) *in vitro*
134 excysted parasites (Figure 2.A). Such controls aimed to differentiate *C. parvum* oocysts from
135 sporozoites and from the background. Flow cytometry analyses were all performed immediately after
136 sample collection on a BD™ LSR II cytometer and data were collected with the BD FACSDiva™
137 Software version 9 (BD Biosciences, Franklin Lakes, USA). Results are expressed as relative
138 percentages of parasites detected as intact oocyst stages in each digestive compartment compared to
139 the corresponding age condition's inoculum.

140 **Sporozoite luciferase activity**

141 The physiological state of *C. parvum* sporozoites was monitored in three independent experiments for
142 the initial parasite suspension and for samples collected regularly from the duodenum, jejunum and

143 ileum compartments during *in vitro* digestions in the TIM-1 system. Immediately after collection, each
144 sample was washed with phosphate-buffered saline (PBS), filtered through a 5 µm membrane
145 (Sartorius AG, Göttingen, Germany) to discard oocysts and empty shells, centrifuged (10000 ×g, 3
146 min, 4°C) and resuspended in PBS. The luciferase activity expressed by the recovered sporozoites was
147 assessed (three replicates for each sample) using the Nano-Glo® Luciferase Assay System (Promega
148 Corporation, Madison, USA). The sporozoites were mixed (v/v) with the Nano-Glo® Luciferase
149 Assay Buffer containing 1:50 of the Nano-Glo® Luciferase Assay Substrate and the luminescence was
150 measured with the GloMax®-Multi Detection System (Promega Corporation, Madison, USA). The
151 luciferase activity expressed by sporozoites collected from the TIM-1 compartments was normalised
152 to the initial parasite suspension for each assay.

153 **Parasite invasion assay**

154 The ability of *C. parvum* sporozoites to invade intestinal epithelial cells was monitored in two
155 independent experiments for samples collected regularly from the small intestinal compartments
156 during *in vitro* digestions. Immediately after collection, each parasite sample was washed with sterile
157 PBS, filtered through a 5 µm membrane (Sartorius AG, Göttingen, Germany) to discard oocysts and
158 empty shells, centrifuged (10000 ×g, 3 min, 4°C) and resuspended into sterile PBS. The recovered
159 sporozoites were immediately used to infect HCT-8 cell monolayers grown to 80% confluence in
160 Nunc™ F96 MicroWell™ white polystyrene plates (Thermo Fisher Scientific, Waltham, USA). After
161 2.5 hours, cells were washed twice with sterile PBS and used to analyse the invasion of parasites (six
162 replicates per sample). The luciferase activity was detected directly from the infected cell monolayers
163 using the Nano-Glo® Luciferase Assay System (Promega Corporation, Madison, USA) and the
164 GloMax®-Multi Detection System as described above. Luciferase activity data were normalised to the
165 luminescence background detected in uninfected cultures.

166 **Parasite RNA extraction**

167 RNA samples were collected on ice from the initial parasite suspension and from gastric (0-20 min) or
168 ileal (120-180 min) effluents during *in vitro* digestions. Samples were then centrifuged (10000 ×g, 5

169 min, 4°C), resuspended into 500 µL TRI Reagent® (Sigma-Aldrich, Saint-Louis, USA) and subjected
170 to 5 cycles of [1 min vortexing - 1 min on ice] after addition of 0.5 mm glass beads. The lysates were
171 centrifuged (10000 ×g, 10 min, 4°C) and the supernatants were mixed with absolute ethanol and
172 transferred to a Zymo-Spin™ IC column (Direct-zol™ RNA Microprep kit, Zymo Research, Irvine,
173 USA). Total RNAs were isolated according to the manufacturer's instructions. Any contaminating
174 genomic DNA was removed using the DNase I Set kit (Zymo Research). RNA was further purified
175 with the RNA Clean & Concentrator™-5 kit (Zymo Research) and concentrations measured using the
176 Qubit™ 2.0 fluorometer using RNA HS assay kit (Thermo Fisher Scientific). RNA quality was
177 assessed using the Agilent 2100 Bioanalyzer system and the RNA 6000 Pico kit (Agilent
178 Technologies, Santa Clara, USA).

179 **RNA-Seq analysis of differentially expressed genes**

180 Library construction and sequencing were performed by Helixio (Biopôle Clermont-Limagne, Saint-
181 Beuzire, France). The RNA library preparation was performed using the QuantSeq 3' mRNA-Seq
182 Library Prep Kit FWD for Illumina (Lexogen, Vienna, Austria). A total of 15 RNA-Seq libraries were
183 generated, corresponding to 3 libraries for each experimental group, and then sequenced with the
184 NextSeq® 500 System (Illumina, San Diego, USA) using a single-read sequencing of 76 bp length
185 configuration. Raw sequence data were assessed for quality using the FastQC v0.11.3 tool (Babraham
186 Institute, Cambridge, UK). Sequenced reads were aligned to the *C. parvum* IOWA-ATCC reference
187 genome (genome assembly ID: ASM1524537v1) using the STAR software (18). The number of
188 sequences reads that mapped the *C. parvum* genome varied between 11 and 14 million per library.
189 Gene counts were determined using the STAR software. The R-based packages DESeq2 (19) and
190 edgeR (20) were used to normalise data, perform descriptive analysis as well as all pairwise
191 comparisons to determine the differentially expressed genes between experimental groups. Clustering
192 of transcriptomic profiles was assessed through a principal-component analysis (PCA) using
193 normalised RNA-Seq data of a set of 2430 filtered genes, for which at least 10 reads were counted in a
194 minimum of three samples. The *P*-values generated during pairwise comparisons were adjusted for
195 multiple testing with the Benjamini-Hochberg procedure which controls for false discovery rate

196 (FDR). Genes were considered to be differentially expressed between two experimental groups at an
197 FDR adjusted P -value < 0.05 . Gene Ontology (GO) (21,22) and KEGG Metabolic Pathway (23–25)
198 enrichment analyses were performed on differentially expressed genes on CryptoDB (26).

199 **Statistical analysis**

200 Graphs and boxplots were generated using GraphPad Prism version 10.2.3 and statistical analyses
201 were performed using R version 4.3.1. Significant differences in luciferase activity and invasion
202 ability data according to time of digestion were tested using a nonparametric analysis of longitudinal
203 data with the R package “nparLD” (27) version 2.2. In case of a significant time effect, pairwise
204 comparisons between time points were calculated with the R package “nparcomp” (28) version 3.0. P
205 < 0.05 was considered statistically significant and indicated by non-corresponding letters (lowercase
206 for the child condition and capitals for the adult condition). The Mann-Whitney non-parametric test
207 was performed to test the effect of treatment (child vs. adult) for each time point and to analyse
208 luciferase data collected from live or heat-killed parasites (Additional file 1), with significant
209 differences indicated as follows: * $P < 0.05$; ** $P < 0.01$; *** $P < 0.001$; **** $P < 0.0001$.

210 **RESULTS**

211 **Parasite excystation kinetics in the simulated upper gastrointestinal tract**

212 To establish the gating strategy, flow cytometry controls were performed during *in vitro* excystation of
213 parasites (Figure 2.A). These controls showed that intact oocysts were abundant before excystation
214 and easily discriminated from empty shells and sporozoites during the process of excystation (when
215 non-filtered). In contrast, intact oocysts were scarcely detected in filtered excysted samples, in which
216 mostly sporozoites could be observed.

217 The same gating strategy was then used to monitor parasite excystation kinetics during child and adult
218 digestions in the TIM-1 system. Time of digestion had an overall significant effect on parasite
219 excystation in both child ($P < 0.0001$) and adult ($P < 0.0001$) conditions. In the simulated stomach

220 compartment, the proportion of intact oocysts (*i.e.*, non-excysted parasites) remained high regardless
 221 of the age condition, with $80.4 \pm 7.2\%$ and $81.4 \pm 10.1\%$ intact oocysts detected at 45 min for child
 222 and adult digestion, respectively (Figure 2.B, Table 1). In contrast, subsequent transit in the duodenal
 223 compartment marked a brutal decrease in the proportion of intact oocysts detected, which dropped to
 224 $4.5 \pm 0.3\%$ and $1.5 \pm 0.3\%$ at 60 min for child and adult condition, respectively. The parasite
 225 excystation further progressed in the small intestine compartments and reached a minimal amount of
 226 intact oocysts detected for both conditions in the ileal compartment by the end of digestion ($1.0 \pm$
 227 0.1% and $0.6 \pm 0.1\%$ at 300 min for the child and the adult digestion, respectively). The quantity of
 228 intact oocysts detected in the child's small intestine was consistently higher when compared to the
 229 adult condition whatever the compartment and time considered (Table 1). Our results suggest that
 230 sporozoites released from excystation in the small intestine would be slightly less abundant in infants
 231 compared to adults.

232 **Table 1.** Percentage of parasites detected as intact oocysts for the child or adult TIM-1 experiments.

Age condition	TIM-1 digestion	0 min Ino	20 min Sto	45 min Stomach	60 min Duo	120 min Jej	180 min Ile	300 min Ile
CHILD	1	100	98.2	93.5	3.8	1.9	1.8	1.1
	2	100	73.5	68.6	4.7	2.6	2.4	0.9
	3	100	86.8	79.0	5.0	2.7	2.6	1.0
ADULT	1	100	101.5	99.5	1.4	1.3	1.2	0.9
	2	100	83.2	64.7	2.0	1.4	1.1	0.6
	3	100	90.1	79.9	1.0	0.7	0.6	0.4

233 The parasite excystation kinetics was analysed by flow cytometry during child or adult digestion in the
 234 TIM-1 system. Samples recovered from the inoculum (Ino) or from the stomach (Sto), duodenum
 235 (Duo), jejunum (Jej) or ileum (Ile) compartments were immediately processed after collection. Values
 236 from three independent child or adult digestion in the TIM-1 system are expressed as relative
 237 percentages of intact oocysts as compared with that of the inoculum for each digestion assay.

238 **Physiological state and invasion ability of *C. parvum* sporozoites collected from the *in***
 239 ***vitro* small intestine**

240 The physiological state of the sporozoites released following excystation in the small intestine of the
 241 TIM-1 system was estimated through analysis of the activity of the luciferase reporter gene that is

242 constitutively expressed by the parasite strain (Figure 3.A). Time of digestion had an overall
243 significant effect on sporozoite luciferase activity in both child ($P < 0.0001$) and adult ($P < 0.0001$)
244 conditions. In the child small intestine, sporozoite relative luciferase activity significantly increased
245 from 38.9 ± 12.1 normalised relative light units (RLUs) in the duodenum at 60 min and 950.5 ± 12.1
246 RLUs in the jejunum at 120 min to a maximum reached at 180 min in the ileum ($2.0 \times 10^4 \pm$
247 4.2×10^3 RLUs; $P < 0.0001$ between 60 min and 180 min and between 120 min and 180 min).
248 During the last two hours of digestion, the relative luciferase activity detected in the child ileal
249 compartment decreased ($7.9 \times 10^3 \pm 1.4 \times 10^3$ RLUs) but remained significantly higher than the
250 one detected in the duodenum and jejunum at the beginning of digestion ($P < 0.0001$ between 60 min
251 and 300 min and between 120 min and 300 min). The luciferase activity kinetics of sporozoites
252 collected from the adult digestions followed the same trend but at a much lower intensity, with a
253 maximum reached of 706.7 ± 80.0 RLUs at 180 min in the ileum. Additionally, the relative luciferase
254 activity expressed by sporozoites was consistently and significantly higher for the child condition
255 when compared to the adult one, whatever the compartments of the small intestine and the time points
256 ($P < 0.0001$ at 60, 120, 180 and 300 min). Controls performed on the *C. parvum* INRAE Nluc strain
257 showed that the luciferase activity measured from excysted parasites was dependent on the quantity (P
258 < 0.01 between 1×10^7 and 1×10^8 excysted parasites) and viability ($P < 0.01$ between live and
259 heat-killed parasites) of parasites present in the sample (Additional file 1). In the TIM-1 small intestine
260 under child condition, fewer sporozoites (Figure 2.B, Table 1) but a significantly higher luciferase
261 activity (Figure 3.A) was detected compared to the adult condition.

262 The invasion ability of Nluc-expressing sporozoites collected and purified from the TIM-1 small
263 intestine was assessed by *in vitro* infection of HCT-8 cell monolayers and subsequent determination of
264 luciferase activity (Figure 3.B). Time of digestion had an overall significant effect on sporozoite
265 ability to invade host cells in both child ($P < 0.0001$) and adult ($P < 0.0001$) conditions. The invasion
266 of HCT-8 monolayers was observed to be low and stable for sporozoites collected from the duodenum
267 at 60 min or from the jejunum at 120 min of both child ($9.3 \times 10^2 \pm 3.4 \times 10^2$ RLUs and
268 $1.4 \times 10^3 \pm 2.5 \times 10^2$ RLUs, respectively) and adult ($3.0 \times 10^2 \pm 1.2 \times 10^2$ RLUs and

269 $4.6 \times 10^2 \pm 1.6 \times 10^2$ RLU, respectively) digestive conditions. The invasion ability was observed
270 to be significantly increased for sporozoites collected at 180 min from the child ileum ($8.0 \times 10^3 \pm$
271 3.0×10^3 RLU; $P < 0.01$ between 180 min and other time points) or the adult ileum ($4.8 \times 10^3 \pm$
272 8.0×10^2 RLU; $P < 0.0001$ between 180 min and other time points). By the end of digestion,
273 parasite invasion dropped to a level comparable to the one observed at 60 min or 120 min, with a
274 relative luminescence of $1.0 \times 10^3 \pm 2.8 \times 10^2$ or $5.1 \times 10^2 \pm 1.3 \times 10^2$ RLU detected for
275 monolayers infected with sporozoites collected at 300 min in the child or adult ileum, respectively.
276 The invasion ability of sporozoites was significantly higher in children compared with adults only at
277 120 min in the jejunum ($P < 0.01$).

278 **Parasite gene expression following child or adult digestion in the TIM-1 model**

279 The parasite transcriptome modifications induced by adult or child digestions in the TIM-1 were
280 determined by whole transcriptome sequencing (RNA-Seq) for gastric (0-20 min) and ileal (120-180
281 min) effluents, and also for the initial inoculum as control. A principal component analysis (PCA) was
282 performed to evaluate the samples' distribution according to their expression profiles. The first (31%)
283 and second (16%) components represented most of the differential expression pattern with a
284 cumulative proportion of 47% (Figure 4.A). This PCA analysis revealed a segregation between
285 samples collected at different time points and from different TIM-1 compartments. The PCA plot
286 showed that all six samples from the ileal effluents were grouped together, and that the three inoculum
287 samples and the six samples from the gastric effluents formed two other distinct groups (*i.e.*, clusters),
288 despite samples 'Inoculum_3' and 'Stomach_Adult2' being more distant from their respective
289 replicates. For each cluster corresponding to samples collected from gastric or ileal effluents, no
290 further segregation by age could be observed, suggesting that most of the variance is explained by
291 time and/or digestive compartment, rather than simulated age (*i.e.*, child vs. adult). Indeed, pairwise
292 comparisons resulted in no or only one gene (Gene ID CPATCC_0017110: unspecified product)
293 whose expression was significantly modified (*i.e.*, showing an adjusted P -value [FDR] < 0.05 and a
294 minimum 2-fold regulation [$\log_2\text{FC} > 1$]) between the two age conditions when effluent was collected
295 in the gastric or in the ileal compartment, respectively (Figure 4.B, Additional files 2 and 3). In

296 contrast, expression profiles were more affected by time and/or digestive compartment, with for
297 example 22 genes whose transcription levels were modified between gastric samples and inoculum for
298 both age conditions, and 83 or 99 genes between gastric and ileal samples for child or adult conditions,
299 respectively. Furthermore, the strongest modulation of the parasite transcriptome was observed
300 between ileal samples and inoculum, with 190 genes whose transcription levels were significantly
301 affected in the adult digestive condition and up to 208 genes in the child.

302 Most of the differentially expressed genes (DEGs) detected in samples collected from the stomach
303 between 0 and 20 min and compared to the inoculum were found upregulated: 18/22 or 20/22 for child
304 or adult, respectively, with 14 genes shared by both age conditions (Figure 4.C, Additional files 4 and
305 5). An analysis of enriched gene ontology (GO) performed on these overexpressed genes in the
306 stomach of the child condition found two significantly enriched GO terms related to cellular
307 components (Additional files 4 and 6.A): ribonucleoprotein complex (FDR = 0.026) and ribosome
308 (FDR = 0.026), both associated with the translation process. Approximately two thirds (*i.e.*, 67.4% or
309 63.6% for child and adult conditions, respectively) of the DEGs identified in ileal samples compared
310 to gastric samples were found downregulated (Figure 4.C, Additional files 7 and 8). Thirty-two
311 significantly downregulated genes are shared by child and adult conditions, among which a gene
312 encoding a myosin motor domain containing protein (Gene ID CPATCC_0009620) showed a 6-fold
313 decrease. One gene encoding an actin protein (Gene ID CPATCC_0025920) showed a 3.8-fold
314 decrease, but only in the child condition. Among downregulated genes, GO enrichment analysis
315 revealed a single significantly enriched GO term related to a molecular function in the adult condition:
316 protein tyrosine/serine/threonine phosphatase activity (FDR = 0.024). Six genes that were found
317 significantly upregulated in the child ileum compared to the child stomach encode putative secreted
318 proteins, of which two are part of the SKSR family (Gene IDs CPATCC_0030860 and
319 CPATCC_0035410) and one is an alpha/beta hydrolase (Gene ID CPATCC_0025460), the latter being
320 also significantly upregulated in the adult condition. The GO enrichment analysis found six
321 significantly enriched GO terms in the child (FDR < 0.05), all related to diverse cellular components
322 (*i.e.*, nuclear or organelle compartments) (Additional files 6.B and 7). The expression of a gene

323 encoding an actin family protein showed a 40-fold significant increase in the adult condition (Gene ID
324 CPATCC_0036850).

325 As mentioned above, the strongest modification of the parasite transcriptome was observed for ileal
326 samples between 120 and 180 min of digestion when compared to the initial inoculum (Figure 4.B,
327 Additional files 9 and 10). For instance, 98 and 83 DEGs were significantly downregulated in child
328 and adult ileum, respectively, with 56 genes shared by both age conditions (Figure 4.C). Among
329 shared downregulated genes, the expression of the gene CPATCC_0009860 encoding the
330 cryptosporidial mucin, also designated as glycoprotein-900 (GP900), was significantly decreased by a
331 4.8-fold. The myosin motor domain containing protein-encoding gene CPATCC_0009620 was also
332 significantly downregulated in the ileum compared to the inoculum (9.7- or 6.8-fold decrease in the
333 child or the adult condition, respectively). Subsequent metabolic pathway enrichment analysis
334 interrogating the KEGG pathway database with significantly downregulated genes highlighted
335 glycolysis/gluconeogenesis as the single significantly enriched pathway in the child ileum (FDR =
336 0.029) (Figure 5.A). The expression of 110 and 107 genes was significantly increased in child and
337 adult ileum, respectively, among which the majority (*i.e.*, 81 genes) was shared by both age conditions
338 (Figure 4.C). For example, four genes encoding putative secreted protein were significantly
339 upregulated in both child and adult ileum, when compared to the inoculum. Among those genes, one
340 relates to the putative secreted alpha/beta hydrolase previously identified (Gene ID
341 CPATCC_0025460) and two belong to the SKSR gene family (CPATCC_0000030 and
342 CPATCC_0030860). GO enrichment analysis performed on significantly upregulated genes
343 highlighted 22 significantly enriched GO terms (FDR < 0.05) shared by child and adult (Figure 5,
344 Additional files 9 and 10). Among these, the top three shared enriched GO terms were associated with
345 cellular components and identified as intracellular structure, intracellular organelle and organelle.
346 Gene expression was shared by both age conditions and associated to 26 or 32 genes out of the 110
347 (23.6%) or 107 (29.9%) significantly upregulated genes detected in the child or the adult condition,
348 respectively. Using the KEGG pathway database, folate biosynthesis was identified as the top one
349 enriched pathway in child (FDR = 0.0008) or adult (FDR = 0.010) ileum compared to the inoculum,

350 and was mostly associated with upregulated helicase-encoding genes. Interestingly, the expression of
351 one gene associated to myosin complex and cytoskeletal motor activity (Gene ID CPATCC_0021030),
352 was highly significantly upregulated by a 1978-fold in the child ileum, compared to the inoculum
353 sample.

354 **DISCUSSION**

355 The goal of our study was to perform a comparative analysis of *C. parvum* infection under the
356 digestive conditions encountered in young children (from 6 months to 2 years) *versus* those in adults.
357 Due to the inherent limitations of *in vivo* experimentation within the host, the investigation of *C.*
358 *parvum* excystation has only been performed to date with highly simplified *in vitro* approaches
359 integrating only a few digestive parameters simultaneously (*e.g.*, temperature, pH) (29). Furthermore,
360 these approaches have never been conducted under finely defined child *vs.* adult digestive conditions,
361 nor combining digestive physicochemical properties with transit dynamism. Based on previous studies
362 on other pathogens (10,12–14,16), we used the dynamic multicompartmental TIM-1 system as a
363 suitable model to monitor *C. parvum* excystation along the simulated human upper gastrointestinal
364 tract of both infant and adult conditions. Our study demonstrates for the first time that most oocysts
365 are found intact in the simulated human stomach compartment 45 min after inoculation in the TIM-1
366 and that the excystation step occurs rapidly and is almost completed within the following 15 min and
367 upon passage in the duodenal compartment. These data suggest that the majority of *C. parvum* oocysts
368 do not undergo excystation until reaching the duodenum, thereby avoiding premature release and
369 subsequent inactivation of the more susceptible sporozoite stages in the gastric acid environment. This
370 is in accordance with the existence of two *Cryptosporidium* lineages that show adaptation to different
371 excystation conditions, one displaying gastric tropism including parasite species that multiply in this
372 gastric acidic environment (*e.g.*, *C. andersoni* and *C. muris*) and one exhibiting intestinal tropism (*e.g.*,
373 *C. parvum* and *C. hominis*) (30). In order to maximise the delivery of sporozoites according to species
374 tropism, excystation is thus activated by different host-derived triggers. In the TIM-1 system,
375 mirroring *in vivo* situations, the excystation of *C. parvum* oocysts might have been triggered first by

376 elevation of the temperature to 37°C upon parasite inoculation into the system, followed by a drastic
377 change in pH upon passage from the acid gastric compartment to the alkaline duodenal one. Previous
378 *in vitro* studies investigating host-derived factors triggering *C. parvum* oocysts excystation have
379 reported that temperature increase and pH change play the most important roles in the transduction of
380 external signals across the oocyst wall to sporozoites (29,31–33). The digestive secretions (*i.e.*, bile
381 salts, trypsin and pancreatic juice) that the duodenal compartment receives in the TIM-1 system might
382 also play a role in *C. parvum* excystation process, although our knowledge of their precise role as
383 excystation triggers or putative synergistic effect is still limited. Interestingly, *in vitro* incubation of
384 oocysts in bile, in particular in sodium taurocholate following exposure to an acid pre-treatment, has
385 been shown to enhance parasite excystation, mimicking transition from the acidic gastric environment
386 to the alkaline small intestine (29,31,34).

387 Our flow cytometry analysis suggests that the excystation rate was slightly more efficient along the
388 simulated small intestine compartments upon adult digestive condition compared to the child one. This
389 could be attributable to specific differences in the physicochemical parameters described for child
390 *versus* adult physiology in a healthy state, which were subsequently implemented into the TIM-1
391 programs (12). For instance, the discrepancy in excystation success may be explained by the slower
392 and less pronounced gastric pH acidification in children (35,36) and/or by the lower concentrations of
393 various secretion components delivered in the child's duodenum, especially of bile salts (37,38)
394 known to enhance excystation (29,31,34).

395 The constitutively expressed luciferase marker was used as an indicator to assess sporozoite
396 physiological state, since the intensity of its robust and sensitive signal correlates directly with the
397 number and viability of parasites (Additional file 1). Taken together, our flow cytometry and
398 luciferase analyses suggest that the highest amount of released sporozoites is present in the simulated
399 ileum, and their physiological state peaks in this compartment at 180 min of digestion, regardless of
400 age conditions. This suggests that *C. parvum* has evolved an excystation process that ensures the
401 accumulation of the maximum number of freshly released sporozoites in the gastrointestinal segment
402 where this species shows the highest tissue tropism *in vivo*. While *C. parvum* has been reported to

403 colonise both proximal intestinal segments and the colon in different hosts (39,40), infections
404 associated with this species are predominantly concentrated in the distal small intestine (41,42). For
405 instance, recent *in vivo* bioluminescent imaging of a Nluc-expressing *C. parvum* strain throughout the
406 intestinal tract of IFN- γ -KO mice clearly showed the parasites to be mainly localised in the ileum
407 section as well as in the caecum (43).

408 Our results also suggest that simulated small intestine of the child condition is associated with fewer
409 sporozoites on the one hand, but a significantly higher sporozoite luciferase activity on the other hand
410 compared to the adult condition. Consequently, sporozoites residing in the intestinal tract of infants
411 could be characterised by a higher viability or be in a less damaged state. In the context of a
412 contamination by the major food- or waterborne pathogen enterohemorrhagic *Escherichia coli* (EHEC
413 O157:H7 serotype), Roussel *et al.* used a similar TIM-1 setup to demonstrate that a higher amount of
414 viable bacterial cells may reach the distal parts of the child's small intestine, compared to those of
415 adults (12). These results might be attributed to less stringent conditions encountered by bacteria or *C.*
416 *parvum* sporozoites in the child's intestinal tract, in regard to the two-fold lower concentration in bile
417 salts and pancreatic secretions described for children compared to adults (37,38,44,45), also
418 reproduced in the TIM-1 model. To our knowledge, the direct impact of various concentrations of
419 duodenal secretions on *C. parvum* sporozoite survival has not yet been investigated. Therefore, we can
420 not exclude that the significantly decreased physiological state observed for the sporozoites released in
421 the adult small intestine may be the result of the detergent properties associated with higher
422 concentrations of duodenal secretions encountered in this environment.

423 We then aimed to investigate whether the higher physiological state of *C. parvum* sporozoites
424 observed in the child intestinal tract could also correlate with an increased infectivity. To this end, the
425 TIM-1 system was combined for the first time with a cell culture assay, wherein we tested the capacity
426 of sporozoites collected from the digestive compartments to invade human intestinal epithelial cells.
427 The invasion assay suggests that sporozoites collected from the ileal compartment at 180 min of
428 digestion have a significantly higher ability to invade HCT-8 cells, compared to other time points.
429 This finding may reflect the slightly higher amount of sporozoites present in the ileum compartment,

430 as compared to the duodenum compartment for instance, but it may also be linked to the significantly
431 higher sporozoites' physiological state and further emphasizes the tropism of *C. parvum* for the ileum *in*
432 *vivo*. Interestingly, when collected from the same TIM-1 compartment, but at the end of the digestion
433 process (300 min of digestion), sporozoites show a decreased luciferase activity and demonstrate a
434 markedly reduced ability to invade host cells. In the literature, *C. parvum* sporozoites have been
435 reported as somewhat fragile (46–48), surviving only for a few hours after release from the much more
436 resilient oocyst stage. Our results are in agreement with this description and suggest that the infectivity
437 potential of these vulnerable parasite stages may decrease drastically in the small intestine lumen if
438 invasion of epithelial cells does not occur quickly after excystation. Our invasion assay shows that,
439 although a lower amount of sporozoites was inoculated to host cells under the child condition (*i.e.*,
440 according to our flow cytometry data), these sporozoites exhibit equivalent or even significantly
441 higher invasion ability compared to the adult condition, most likely due to their “better” physiological
442 state. Thus, our results suggest that age-related variability in digestive physicochemical parameters
443 may modulate different features of sporozoite physiology, and therefore participate in higher
444 susceptibility of young children to *C. parvum* infection compared to adults.

445 In this study, we also aimed to characterise the modulation of the *C. parvum* gene expression in
446 response to the various digestive physicochemical parameters encountered by the parasite in two
447 different compartments of the child or adult gastrointestinal tract. Intriguingly, our results revealed
448 that the parasite transcriptome is almost exclusively affected by the time and/or compartment of
449 digestion in the TIM-1, rather than by the simulated age (*i.e.*, child *vs.* adult). This observation
450 suggests that parasite gene expression is predominantly governed by the succession of shifts in
451 digestive environmental conditions and the duration of digestion, rather than by more subtle
452 physicochemical specificities associated with age condition. In contrast, previous RT-qPCR analyses
453 performed on TIM-1 gastric and ileal effluents have shown that the expression of major EHEC
454 O157:H7 bacterial virulence genes was significantly higher under child digestive conditions,
455 compared to the adult ones (12). Regarding *C. parvum*, although differences in digestive
456 physicochemical properties between infants and adults may influence the amount, physiological state

457 and invasiveness of sporozoites released in the small intestine, they may not be associated with
458 significant modulation of parasite genes associated with virulence.

459 Transcriptomic analysis performed on TIM-1 gastric effluents collected within the initial twenty
460 minutes of digestion detected a low number of DEGs between stomach and inoculum samples,
461 predominantly exhibiting upregulation. In this digestive compartment, where most parasites were
462 found as intact oocysts, enrichment of upregulated genes associated with gene expression and
463 translation was detected. Similarly, previous transcriptomic analysis has revealed that the *C. parvum*
464 oocyst stage is highly active in protein synthesis, as evidenced by high transcripts levels of parasite
465 genes involved in ribosome biogenesis, transcription and translation (49).

466 We also analysed the *C. parvum* transcriptome collected from TIM-1 ileal effluents between 120 and
467 180 min of digestion, when the vast majority of parasites are found as released sporozoites compared
468 to the stomach compartment. Our RNA-Seq analysis revealed that the sporozoite-enriched
469 transcriptome exhibited much greater modulation in the ileum compared to the stomach, with
470 approximately 25% of upregulated genes associated with gene expression, nucleus or intracellular
471 structures and organelles. KEGG analysis highlighted the glycolysis/gluconeogenesis as a significantly
472 downregulated pathway in parasites collected from ileal effluents. Although *C. parvum* may possess a
473 remnant mitochondrion, it lacks the Krebs cycle and the cytochrome-based respiration, therefore
474 relying mainly, if not only, on glycolysis for ATP production (50). Glycolysis-related genes are known
475 to be highly expressed in intracellular developmental stages (51), supporting *C. parvum* replication
476 inside host cells. While some of their related products have also been detected in the sporozoite
477 proteome (52), they were found under-represented in this repertoire in another proteomic study (53).

478 Previous transcriptomic analysis has shown that, in contrast to intracellular developmental stages, *C.*
479 *parvum* extracellular stages (*i.e.*, oocysts and sporozoites) express a wider range of genes encoding
480 specialised functions (54), with few identified orthologs outside or related protozoan organisms. Like
481 other apicomplexan parasites, the polarised *C. parvum* sporozoites harbour unique apical secretory
482 organelles involved in attachment, invasion, penetration and maintenance of the parasite within the
483 host cell, (*i.e.*, micronemes, dense granules, small granules and a single rhoptry), as well as the

484 canonical glideosome dependent on actin and myosin providing parasite gliding motility (55–57).
485 Accordingly, the expression of several parasite genes associated with the latter apicomplexan feature,
486 particularly the myosin complex and cytoskeletal motor activity, was significantly modulated in the
487 sporozoite-enriched fractions collected from the TIM-1 ileal effluents. While two of these genes (Gene
488 IDs CPATCC_0009620 and CPATCC_0025920) showed a moderate downregulation in these
489 samples, two other encoding a protein from the actin family (Gene ID CPATCC_0036850) and a
490 myosin motor domain containing protein (Gene ID CPATCC_0021030) were characterised by a
491 tremendous 40- or ~ 2000-fold upregulation, respectively. Alongside this marked regulation of genes
492 potentially related to parasite gliding motility, the expression of genes encoding putative secreted
493 proteins was significantly modulated in ileal effluents. For instance, the expression levels of the
494 mucin-like glycoprotein GP900 (Gene ID CPATCC_0009860) were significantly downregulated in
495 our ileal sporozoite-enriched samples. Stored in the sporozoite micronemes and previously
496 hypothesised to be involved in attachment and/or invasion (58), the immunodominant protein GP900
497 has recently been shown to enter the secretory pathway after excystation, where its short cytoplasmic
498 domain is cleaved before discharge of the cleaved form to the extracellular space, suggesting a
499 lubrication role during sporozoite invasion (59). Finally, six genes encoding putative secreted proteins
500 were significantly upregulated in the TIM-1 ileal effluents, consistent with the past detection of
501 several proteins associated with extracellular protein secretion in the protein repertoire of *C. parvum*
502 sporozoites (52,53). Apart from a predicted hydrolase, the function of these putative secreted proteins
503 is not yet known. Interestingly, three of these genes are predicted to encode proteins belonging to the
504 SKSR family (Gene IDs CPATCC_0030860, CPATCC_0000030 and CPATCC_0035410). This
505 *Cryptosporidium*-specific multigene family comprises most highly polymorphic and subtelomeric
506 genes encoding secreted proteins harbouring a signal peptide and SK and SR repeats (60). Although
507 present in all major human-infecting *Cryptosporidium* species, differences in the presence or absence,
508 as well as in the copy numbers of this subtelomeric gene family, were recently identified between
509 sequenced *Cryptosporidium* genomes by comparative genomic analyses, similarly to two other
510 families encoding the MEDLE secretory proteins, named after their conserved sequence motif at the
511 C-terminus, and insulinase-like proteases (61–66). Recent findings identified SKSR1 as a member of

512 the secretory proteins (67) in the newly identified small granules organelles (57). Additionally, SKSR1
513 was shown to be secreted into the parasite-host interface (*i.e.*, parasitophorous vacuole membrane and
514 feeder organelle) and to be important for *C. parvum* pathogenicity, suggesting that it may act as a
515 virulence factor through regulating host responses (67). More comparative studies are needed to fully
516 elucidate the function of all SKSR members, since gene gains and losses of this subtelomeric gene
517 family are suggested to contribute to differences in pathogenicity and host specificity in
518 *Cryptosporidium* populations.

519 CONCLUSIONS

520 Being one of the most common causes of infectious moderate-to-severe diarrhoea in young children,
521 cryptosporidiosis is an important contributor to early childhood mortality in low-resource settings.
522 Increased susceptibility of infants and toddlers to *Cryptosporidium* can be attributed to immature
523 immune status in this age group. Using the sophisticated TIM-1 *in vitro* gastrointestinal model, we
524 showed that the digestive physicochemical parameters encountered in the child digestive tract could be
525 associated with fewer, however potentially more active and invasive sporozoites released. Our results
526 suggest that age-mediated variation in the human gastrointestinal physiology could also partially
527 explain why young individuals are more at risk. The link between specificities of the child digestive
528 tract and disease is complex. Understanding the interactions between *C. parvum* infection and various
529 digestive components of young individuals, including physicochemical parameters, mucus barrier, and
530 microbiota, can provide us with a more accurate picture of children susceptibility, and possible
531 valuable information towards new treatment strategies.

532 LIST OF ABBREVIATIONS

533 ATP: Adenosine triphosphate

534 *C. andersoni*: *Cryptosporidium andersoni*

535 *C. hominis*: *Cryptosporidium hominis*

- 536 *C. muris*: *Cryptosporidium muris*
- 537 *C. parvum*: *Cryptosporidium parvum*
- 538 DEG: Differentially expressed gene
- 539 DNA: Deoxyribonucleic acid
- 540 DNase: Deoxyribonuclease
- 541 *E. coli*: *Escherichia coli*
- 542 EHEC O157:H7: Enterohemorrhagic *Escherichia coli* serotype O157:H7
- 543 FBS: Fetal bovine serum
- 544 FDR: False discovery rate
- 545 GO: Gene ontology
- 546 GP900: Glycoprotein-900
- 547 IFN- γ : Interferon gamma
- 548 KEGG: Kyoto encyclopedia of genes and genomes
- 549 KO: Knock-out
- 550 Nluc: Nanoluciferase
- 551 PBS: Phosphate-buffered saline
- 552 PCA: Principal component analysis
- 553 RLU: Relative light unit
- 554 RNA: Ribonucleic acid
- 555 RNA-Seq: RNA sequencing
- 556 RPMI: Roswell Park Memorial Institute
- 557 SEM: Standard error of the mean
- 558 TIM-1: TNO (Toegepast Natuurwetenschappelijk Onderzoek) gastrointestinal model-1

559 **DECLARATIONS**

560 **Ethics approval and consent to participate**

561 Not applicable

562 **Consent for publication**

563 Not applicable

564 **Availability of data and materials**

565 The datasets generated and analysed during the current study are available in the GEO repository
566 database, under accession number GSE271211
567 (<https://www.ncbi.nlm.nih.gov/geo/query/acc.cgi?&acc=GSE271211>).

568 **Competing interests**

569 The authors declare that they have no competing interests.

570 **Funding**

571 This research was supported by the INRAE Animal Health division and by the Laboratoire
572 d'Excellence (LabEx) ParaFrap (ANR-11-LABX-0024).

573 **Author's contributions**

574 JT, LE-M, SB-D and SL-L designed the project and the experiments. JT, LE-M, SC, AS, SD, CM and
575 SL-L performed the experiments. JT and AS produced and purified the oocysts of the *C. parvum*
576 INRAE Nluc strain. LE-M, SC, SD and CM performed the *in vitro* digestions. SL-L performed the
577 flow cytometry analysis with the help of CB. JT performed the sporozoite luciferase activity and the
578 cell culture experiments. AS performed the parasite RNA extractions. JT and GS analysed the RNA-
579 Seq data. JT, LE-M, GS, FL, SB-D and SL-L interpreted the experimental work. JT, LE-M, FL, SB-D

580 and SL-L secured funding. JT, LE-M, SB-D and SL-L wrote the paper with editorial support and
581 comments from all other authors. All authors read and approved the final version of the manuscript.

582 **Acknowledgments**

583 We would like to thank the Helixio company for the mRNA sequencing and bioinformatics analysis.

584 We are also very grateful to Elise Courtot (UMR ISP, INRAE) for her help on statistical analysis.

585 **REFERENCES**

- 586 1. Checkley W, White AC, Jaganath D, Arrowood MJ, Chalmers RM, Chen XM, et al. A review of
587 the global burden, novel diagnostics, therapeutics, and vaccine targets for *Cryptosporidium*. *Lancet*
588 *Infect Dis*. 2015;15(1):85–94.
- 589 2. Kotloff KL, Nataro JP, Blackwelder WC, Nasrin D, Farag TH, Panchalingam S, et al. Burden and
590 aetiology of diarrhoeal disease in infants and young children in developing countries (the Global
591 Enteric Multicenter Study, GEMS): a prospective, case-control study. *Lancet*.
592 2013;382(9888):209–22.
- 593 3. Platts-Mills JA, Babji S, Bodhidatta L, Gratz J, Haque R, Havt A, et al. Pathogen-specific burdens
594 of community diarrhoea in developing countries: a multisite birth cohort study (MAL-ED). *Lancet*
595 *Glob Health*. 2015;3(9):e564–575.
- 596 4. Mølbak K, Højlyng N, Gottschau A, Sá JC, Ingholt L, da Silva AP, et al. Cryptosporidiosis in
597 infancy and childhood mortality in Guinea Bissau, west Africa. *BMJ*. 1993;307(6901):417–20.
- 598 5. Khalil IA, Troeger C, Rao PC, Blacker BF, Brown A, Brewer TG, et al. Morbidity, mortality, and
599 long-term consequences associated with diarrhoea from *Cryptosporidium* infection in children
600 younger than 5 years: a meta-analysis study. *Lancet Glob Health*. 2018;6(7):e758–68.
- 601 6. Shirley DAT, Moonah SN, Kotloff KL. Burden of disease from cryptosporidiosis. *Curr Opin Infect*
602 *Dis*. 2012;25(5):555–63.
- 603 7. English ED, Guérin A, Tandel J, Striepen B. Live imaging of the *Cryptosporidium parvum* life
604 cycle reveals direct development of male and female gametes from type I meronts. *PLoS Biol*.
605 2022;20(4):e3001604.
- 606 8. Laurent F, Lacroix-Lamandé S. Innate immune responses play a key role in controlling infection of
607 the intestinal epithelium by *Cryptosporidium*. *Int J Parasitol*. 2017;47(12):711–21.
- 608 9. Kaye JL. Review of paediatric gastrointestinal physiology data relevant to oral drug delivery. *Int J*
609 *Clin Pharm*. 2011;33(1):20–4.
- 610 10. Uriot O, Chalancon S, Mazal C, Etienne-Mesmin L, Denis S, Blanquet-Diot S. Use of the dynamic
611 TIM-1 model for an in-depth understanding of the survival and virulence gene expression of Shiga
612 toxin-producing *Escherichia coli* in the human stomach and small intestine. *Methods Mol Biol*.
613 2021;2291:297–315.

- 614 11. Miszczucha SD, Thévenot J, Denis S, Callon C, Livrelli V, Alric M, et al. Survival of *Escherichia*
615 *coli* O26:H11 exceeds that of *Escherichia coli* O157:H7 as assessed by simulated human digestion
616 of contaminated raw milk cheeses. *Int J Food Microbiol.* 2014;172:40–8.
- 617 12. Roussel C, Cordonnier C, Galia W, Le Goff O, Thévenot J, Chalancon S, et al. Increased EHEC
618 survival and virulence gene expression indicate an enhanced pathogenicity upon simulated pediatric
619 gastrointestinal conditions. *Pediatr Res.* 2016;80(5):734–43.
- 620 13. Roussel C, De Paepe K, Galia W, De Bodt J, Chalancon S, Leriche F, et al. Spatial and temporal
621 modulation of enterotoxigenic *E. coli* H10407 pathogenesis and interplay with microbiota in human
622 gut models. *BMC Biol.* 2020;18(1):141.
- 623 14. Roussel C, De Paepe K, Galia W, de Bodt J, Chalancon S, Denis S, et al. Multi-targeted properties
624 of the probiotic *Saccharomyces cerevisiae* CNCM I-3856 against enterotoxigenic *Escherichia coli*
625 (ETEC) H10407 pathogenesis across human gut models. *Gut Microbes.* 2021;13(1):1953246.
- 626 15. Cavestri C, Savard P, Fliss I, Emond-Rhéault JG, Hamel J, Kukavica-Ibrulj I, et al. *Salmonella*
627 *enterica* subsp. *enterica* virulence potential can be linked to higher survival within a dynamic in
628 vitro human gastrointestinal model. *Food Microbiol.* 2022;101:103877.
- 629 16. Sauvaitre T, Van Landuyt J, Durif C, Roussel C, Sivignon A, Chalancon S, et al. Role of mucus-
630 bacteria interactions in Enterotoxigenic *Escherichia coli* (ETEC) H10407 virulence and interplay
631 with human microbiome. *NPJ Biofilms Microbiomes.* 2022;8(1):86.
- 632 17. Swale C, Bougdour A, Gnahoui-David A, Tottey J, Georgeault S, Laurent F, et al. Metal-captured
633 inhibition of pre-mRNA processing activity by CPSF3 controls *Cryptosporidium* infection. *Sci*
634 *Transl Med.* 2019;11(517):eaax7161.
- 635 18. Dobin A, Davis CA, Schlesinger F, Drenkow J, Zaleski C, Jha S, et al. STAR: ultrafast universal
636 RNA-seq aligner. *Bioinformatics.* 2013;29(1):15–21.
- 637 19. Love MI, Huber W, Anders S. Moderated estimation of fold change and dispersion for RNA-seq
638 data with DESeq2. *Genome Biol.* 2014;15(12):550.
- 639 20. Robinson MD, McCarthy DJ, Smyth GK. edgeR: a Bioconductor package for differential
640 expression analysis of digital gene expression data. *Bioinformatics.* 2010;26(1):139–40.
- 641 21. Ashburner M, Ball CA, Blake JA, Botstein D, Butler H, Cherry JM, et al. Gene ontology: tool for
642 the unification of biology. The Gene Ontology Consortium. *Nat Genet.* 2000;25(1):25–9.
- 643 22. Gene Ontology Consortium, Aleksander SA, Balhoff J, Carbon S, Cherry JM, Drabkin HJ, et al.
644 The Gene Ontology knowledgebase in 2023. *Genetics.* 2023;224(1):iyad031.
- 645 23. Kanehisa M, Goto S. KEGG: kyoto encyclopedia of genes and genomes. *Nucleic Acids Res.*
646 2000;28(1):27–30.
- 647 24. Kanehisa M. Toward understanding the origin and evolution of cellular organisms. *Protein Sci.*
648 2019;28(11):1947–51.
- 649 25. Kanehisa M, Furumichi M, Sato Y, Kawashima M, Ishiguro-Watanabe M. KEGG for taxonomy-
650 based analysis of pathways and genomes. *Nucleic Acids Research.* 2023;51(1):587–D592.
- 651 26. Heiges M, Wang H, Robinson E, Aurrecochea C, Gao X, Kaluskar N, et al. CryptoDB: a
652 *Cryptosporidium* bioinformatics resource update. *Nucleic Acids Res.* 2006;34:419–22.

- 653 27. Noguchi K, Gel YR, Brunner E, Konietzschke F. nparLD: An R Software Package for the
654 Nonparametric Analysis of Longitudinal Data in Factorial Experiments. *Journal of Statistical*
655 *Software*. 2012;50:1–23.
- 656 28. Konietzschke F, Placzek M, Schaarschmidt F, Hothorn LA. nparcomp: An R Software Package for
657 Nonparametric Multiple Comparisons and Simultaneous Confidence Intervals. *Journal of Statistical*
658 *Software*. 2015;64:1–17.
- 659 29. Smith HV, Nichols RAB, Grimason AM. Cryptosporidium excystation and invasion: getting to the
660 guts of the matter. *Trends Parasitol*. 2005;21(3):133–42.
- 661 30. Widmer G, Klein P, Bonilla R. Adaptation of Cryptosporidium oocysts to different excystation
662 conditions. *Parasitology*. 2007;134(11):1583–8.
- 663 31. Robertson LJ, Campbell AT, Smith HV. In vitro excystation of Cryptosporidium parvum.
664 *Parasitology*. 1993;106:13–9.
- 665 32. Forney JR, Yang S, Healey MC. Protease activity associated with excystation of Cryptosporidium
666 parvum oocysts. *J Parasitol*. 1996;82(6):889–92.
- 667 33. Okhuysen PC, Chappell CL, Kettner C, Sterling CR. Cryptosporidium parvum
668 metalloaminopeptidase inhibitors prevent in vitro excystation. *Antimicrob Agents Chemother*.
669 1996;40(12):2781–4.
- 670 34. King BJ, Keegan AR, Phillips R, Fanok S, Monis PT. Dissection of the hierarchy and synergism of
671 the bile derived signal on Cryptosporidium parvum excystation and infectivity. *Parasitology*.
672 2012;139(12):1533–46.
- 673 35. Omari TI, Davidson GP. Multipoint measurement of intragastric pH in healthy preterm infants.
674 *Arch Dis Child Fetal Neonatal Ed*. 2003;88(6):517–20.
- 675 36. Koziolok M, Grimm M, Becker D, Iordanov V, Zou H, Shimizu J, et al. Investigation of pH and
676 Temperature Profiles in the GI Tract of Fasted Human Subjects Using the Intellicap® System. *J*
677 *Pharm Sci*. 2015;104(9):2855–63.
- 678 37. Challacombe DN, Edkins S, Brown GA. Duodenal bile acids in infancy. *Arch Dis Child*.
679 1975;50(11):837–43.
- 680 38. Vertzoni M, Archontaki H, Reppas C. Determination of intraluminal individual bile acids by
681 HPLC with charged aerosol detection. *J Lipid Res*. 2008;49(12):2690–5.
- 682 39. Vítovec J, Koudela B. Pathogenesis of intestinal cryptosporidiosis in conventional and gnotobiotic
683 piglets. *Vet Parasitol*. 1992;43(1–2):25–36.
- 684 40. Kelly P, Makumbi FA, Carnaby S, Simjee AE, Farthing MJG. Variable distribution of
685 Cryptosporidium parvum in the intestine of AIDS patients revealed by polymerase chain reaction.
686 *Eur J Gastroenterol Hepatol*. 1998;10(10):855.
- 687 41. Current WL, Garcia LS. Cryptosporidiosis. *Clin Microbiol Rev*. 1991;4(3):325–58.
- 688 42. de Graaf DC, Vanopdenbosch E, Ortega-Mora LM, Abbassi H, Peeters JE. A review of the
689 importance of cryptosporidiosis in farm animals. *Int J Parasitol*. 1999;29(8):1269–87.
- 690 43. Gallego-Lopez GM, Mendoza Cavazos C, Tibabuzo Perdomo AM, Garfoot AL, O'Connor RM,
691 Knoll LJ. Dual transcriptomics to determine gamma interferon-independent host response to
692 intestinal Cryptosporidium parvum infection. *Infect Immun*. 2022;90(2):e0063821.

- 693 44. Delachaume-Salem E, Sarles H. [Normal human pancreatic secretion in relation to age]. Biol
694 Gastroenterol (Paris). 1970;2:135-46.
- 695 45. Kalantzi L, Goumas K, Kalioras V, Abrahamsson B, Dressman JB, Reppas C. Characterization of
696 the human upper gastrointestinal contents under conditions simulating
697 bioavailability/bioequivalence studies. Pharm Res. 2006;23(1):165-76.
- 698 46. Arrowood MJ. In vitro cultivation of cryptosporidium species. Clin Microbiol Rev.
699 2002;15(3):390-400.
- 700 47. Matsubayashi M, Ando H, Kimata I, Nakagawa H, Furuya M, Tani H, et al. Morphological
701 changes and viability of *Cryptosporidium parvum* sporozoites after excystation in cell-free culture
702 media. Parasitology. 2010;137(13):1861-6.
- 703 48. Castellanos-Gonzalez A, Perry N, Nava S, White AC. Preassembled single-stranded RNA-
704 Argonaute complexes: a novel method to silence genes in *Cryptosporidium*. J Infect Dis.
705 2016;213(8):1307-14.
- 706 49. Zhang H, Guo F, Zhou H, Zhu G. Transcriptome analysis reveals unique metabolic features in the
707 *Cryptosporidium parvum* Oocysts associated with environmental survival and stresses. BMC
708 Genomics. 2012;13:647.
- 709 50. Abrahamsen MS, Templeton TJ, Enomoto S, Abrahante JE, Zhu G, Lancto CA, et al. Complete
710 genome sequence of the apicomplexan, *Cryptosporidium parvum*. Science. 2004;304(5669):441-5.
- 711 51. Mauzy MJ, Enomoto S, Lancto CA, Abrahamsen MS, Rutherford MS. The *Cryptosporidium*
712 *parvum* transcriptome during in vitro development. PLoS One. 2012;7(3):e31715.
- 713 52. Snelling WJ, Lin Q, Moore JE, Millar BC, Tosini F, Pozio E, et al. Proteomics analysis and protein
714 expression during sporozoite excystation of *Cryptosporidium parvum* (Coccidia, Apicomplexa).
715 Mol Cell Proteomics. 2007;6(2):346-55.
- 716 53. Sanderson SJ, Xia D, Prieto H, Yates J, Heiges M, Kissinger JC, et al. Determining the protein
717 repertoire of *Cryptosporidium parvum* sporozoites. Proteomics. 2008;8(7):1398-414.
- 718 54. Matos LVS, McEvoy J, Tzipori S, Bresciani KDS, Widmer G. The transcriptome of
719 *Cryptosporidium* oocysts and intracellular stages. Sci Rep. 2019;9(1):7856.
- 720 55. Wetzel DM, Schmidt J, Kuhlenschmidt MS, Dubey JP, Sibley LD. Gliding motility leads to active
721 cellular invasion by *Cryptosporidium parvum* sporozoites. Infect Immun. 2005;73(9):5379-87.
- 722 56. Guérin A, Striepen B. The biology of the intestinal intracellular parasite *Cryptosporidium*. Cell
723 Host Microbe. 2020;28(4):509-15.
- 724 57. Guérin A, Strelau KM, Barylyuk K, Wallbank BA, Berry L, Crook OM, et al. *Cryptosporidium*
725 uses multiple distinct secretory organelles to interact with and modify its host cell. Cell Host
726 Microbe. 2023;31(4):650-664.e6.
- 727 58. Barnes DA, Bonnin A, Huang JX, Gousset L, Wu J, Gut J, et al. A novel multi-domain mucin-like
728 glycoprotein of *Cryptosporidium parvum* mediates invasion. Mol Biochem Parasitol.
729 1998;96(1):93-110.
- 730 59. Li X, Yin J, Wang D, Gao X, Zhang Y, Wu M, et al. The mucin-like, secretory type-I
731 transmembrane glycoprotein GP900 in the apicomplexan *Cryptosporidium parvum* is cleaved in the
732 secretory pathway and likely plays a lubrication role. Parasit Vectors. 2022;15(1):170.

- 733 60. Widmer G, Carmena D, Kváč M, Chalmers RM, Kissinger JC, Xiao L, et al. Update on
734 *Cryptosporidium* spp.: highlights from the Seventh International Giardia and *Cryptosporidium*
735 Conference. *Parasite*. 2020;27:14.
- 736 61. Guo Y, Tang K, Rowe LA, Li N, Roellig DM, Knipe K, et al. Comparative genomic analysis
737 reveals occurrence of genetic recombination in virulent *Cryptosporidium hominis* subtypes and
738 telomeric gene duplications in *Cryptosporidium parvum*. *BMC Genomics*. 2015;16(1):320.
- 739 62. Isaza JP, Galván AL, Polanco V, Huang B, Matveyev AV, Serrano MG, et al. Revisiting the
740 reference genomes of human pathogenic *Cryptosporidium* species: reannotation of *C. parvum* Iowa
741 and a new *C. hominis* reference. *Sci Rep*. 2015;5:16324.
- 742 63. Feng Y, Li N, Roellig DM, Kelley A, Liu G, Amer S, et al. Comparative genomic analysis of the
743 IId subtype family of *Cryptosporidium parvum*. *Int J Parasitol*. 2017;47(5):281–90.
- 744 64. Xu Z, Li N, Guo Y, Feng Y, Xiao L. Comparative genomic analysis of three intestinal species
745 reveals reductions in secreted pathogenesis determinants in bovine-specific and non-pathogenic
746 *Cryptosporidium* species. *Microb Genom*. 2020;6(6):e000379.
- 747 65. Wang T, Guo Y, Roellig DM, Li N, Santín M, Lombard J, et al. Sympatric recombination in
748 zoonotic *Cryptosporidium* leads to emergence of populations with modified host preference. *Mol*
749 *Biol Evol*. 2022;39(7):msac150.
- 750 66. Li J, Li N, Roellig DM, Zhao W, Guo Y, Feng Y, et al. High subtelomeric GC content in the
751 genome of a zoonotic *Cryptosporidium* species. *Microb Genom*. 2023;9(7):mgen001052.
- 752 67. He W, Sun L, Hou T, Yang Z, Yang F, Wang T, et al. SKSR1 identified as key virulence factor in
753 *Cryptosporidium* by genetic crossing. *BioRxiv*. 2024;(577707).

754

755 **FIGURE 1**

756 **Title.** TIM-1 experimental set-up and analysis.

757 **Legend.** The left side shows a picture of the TIM-1 system composed of four successive
758 compartments simulating the human stomach and the three parts of the small intestine (*i.e.*, the
759 duodenum, jejunum and ileum) mimicking the main physicochemical parameters of human
760 gastrointestinal digestion. Digestion experiments were performed to reproduce an adult or an infant
761 (from 6 months old to 2 years old) ingesting a glass of water contaminated with 1×10^8 oocysts of
762 the *C. parvum* INRAE Nluc strain. On the right side, sampling times (minutes) are indicated when
763 samples were taken either directly from each compartment (for flow cytometry, sporozoite luciferase
764 activity and invasion assay); or indirectly by pooling the gastric effluents when the stomach
765 compartment was solely used, or the ileal effluents when the entire TIM-1 system was used (for RNA

766 sequencing). Digestions were run in triplicate. Created with BioRender.com (Agreement number:
767 JH26ZFM4TU).

768 **FIGURE 2**

769 **Title.** *Cryptosporidium parvum* excystation in the human *in vitro* upper gastrointestinal tract.

770 **Legend.** (A) Flow cytometry gating strategy on forward-angle light scatter/side-angle light scatter
771 established during *in vitro* excystation of parasites, allowing detection of intact oocysts, empty oocyst
772 shells and sporozoites. Created with BioRender.com (Agreement number: FF26ZFMVSM). (B)
773 Parasite excystation during child or adult digestion in the TIM-1 system. Cytograms obtained for one
774 representative experiment for the child or the adult digestion at 45 min in the stomach and at 60 min in
775 the duodenum show the timing when excystation occurs in the *in vitro* gastrointestinal tract.

776 **FIGURE 3**

777 **Title.** Physiological state and invasion ability of *Cryptosporidium parvum* sporozoites collected from
778 the TIM-1 system.

779 **Legend.** (A) Luciferase activity expressed by *C. parvum* sporozoites collected from the duodenal
780 (Duo), jejunal (Jej) or ileal (Ile) TIM-1 compartments during child (purple) or adult (dark blue)
781 digestion. Boxplots depict the relative luminescence of sporozoites compared with that of the
782 inoculum for each digestion assay. For each age condition, significant differences ($P < 0.05$) between
783 time points are indicated by non-corresponding letters (purple lowercase for child digestion and blue
784 capitals for adult digestion). For each time point, significant differences between age conditions are
785 indicated in black as follows: **** $P < 0.0001$. (B) Invasion assay. *C. parvum* sporozoites were
786 allowed to infect HCT-8 monolayers for 2.5 h before evaluation of luminescence intensity. Boxplots
787 depict the luminescence measured in infected cells from which the luciferase background measured in
788 non-infected cells has been removed. For each age condition, significant differences ($P < 0.01$ or $P <$
789 0.001 for child or adult, respectively) between time points are indicated by non-corresponding letters

790 (purple lowercase for child digestion and blue capitals for adult digestion). For each time point,
791 significant differences between age conditions are indicated in black as follows: ** $P < 0.01$.

792 **FIGURE 4**

793 **Title.** RNA-Seq analysis of *C. parvum* genes in TIM-1 samples.

794 **Legend.** (A) Principal component analysis of RNA-Seq samples investigating gene expression
795 changes in *C. parvum* parasites collected in the inoculum ($t = 0$ min), or in gastric (0-20 min) or ileal
796 effluents (120-180 min) during the simulated child or adult digestions in the TIM-1. PCA was
797 performed using normalised RNA-Seq data of a set of 2430 filtered genes. (B) Number of
798 differentially expressed genes (DEGs) between pairwise comparisons. All DEGs show an adjusted P -
799 value < 0.05 and a minimal regulation of 2-fold ($\log_2FC > 1$). (C) Number of upregulated (green) or
800 downregulated (orange) genes between samples collected from different TIM-1 compartments in both
801 child and adult conditions. The number of DEGs shared by age conditions is shown in brackets and
802 with the dotted filling pattern.

803 **FIGURE 5**

804 **Title.** Enrichment analysis on *C. parvum* genes differentially expressed in the ileal compartment.

805 **Legend.** The Gene Ontology and KEGG enrichment analysis was performed on genes that were
806 significantly up- or downregulated in the ileal effluents compared with the inoculum. The number of
807 genes associated with each significantly enriched (*i.e.*, showing a Benjamini-Hochberg-adjusted P -
808 value or $FDR < 0.05$) GO term or KEGG pathway is displayed for the child (A) or the adult (B)
809 conditions. The three GO term categories named 'Biological process', 'Cellular component' and
810 'Molecular function' are represented by blue, green or orange bars, respectively. The KEGG
811 Metabolic pathways are represented by grey bars. The GO terms or KEGG pathway shared by both
812 age conditions are indicated by a star.

813 **ADDITIONAL FILE 1**

814 **File format.** Figure (.pdf)

815 **Title of data.** Luciferase activity expressed by live or heat-killed *C. parvum* INRAE Nluc parasites.

816 **Description of data.** Luciferase activity expressed by live or heat-killed *C. parvum* INRAE Nluc
817 parasites. Luciferase activity was measured in live (*i.e.*, maintained at room temperature for 30 min,
818 blue dots) or heat-killed (*i.e.*, maintained at 60°C for 30 min, red dots) *C. parvum* INRAE Nluc
819 parasites, following excystation of 1×10^7 oocysts or 1×10^6 oocysts. Individual values from five
820 independent experiments are represented. Significant differences between groups determined by
821 Mann-Whitney non-parametric test are indicated as follows: ** $P < 0.01$. Cp, *Cryptosporidium*
822 *parvum*. RT, room temperature.

823 **ADDITIONAL FILE 2**

824 **File format.** Excel spreadsheet (.xls)

825 **Title of data.** RNA-Seq Stomach Adult vs Stomach Child.

826 **Description of data.** Differentially expressed genes determined by RNA-sequencing between samples
827 collected in gastric effluents of adult and gastric effluents of child, and results from enrichment
828 analyses performed on significantly upregulated or downregulated genes.

829 **ADDITIONAL FILE 3**

830 **File format.** Excel spreadsheet (.xls)

831 **Title of data.** RNA-Seq Ileal Adult vs Ileal Child.

832 **Description of data.** Differentially expressed genes determined by RNA-sequencing between samples
833 collected in ileal effluents of adult and ileal effluents of child, and results from enrichment analyses
834 performed on significantly upregulated or downregulated genes.

835 **ADDITIONAL FILE 4**

836 **File format.** Excel spreadsheet (.xls)

837 **Title of data.** RNA-Seq Stomach Child vs Inoculum.

838 **Description of data.** Differentially expressed genes determined by RNA-sequencing between samples
839 collected in gastric effluents of child and inoculum, and results from enrichment analyses performed
840 on significantly upregulated or downregulated genes.

841 **ADDITIONAL FILE 5**

842 **File format.** Excel spreadsheet (.xls)

843 **Title of data.** RNA-Seq Stomach Adult vs Inoculum.

844 **Description of data.** Differentially expressed genes determined by RNA-sequencing between samples
845 collected in gastric effluents of adult and inoculum, and results from enrichment analyses performed
846 on significantly upregulated or downregulated genes.

847 **ADDITIONAL FILE 6**

848 **File format.** Figure (.pdf)

849 **Title of data.** Enrichment analysis on *C. parvum* genes differentially expressed in the stomach
850 compared to the inoculum (A) or in the ileum compared to the stomach (B).

851 **Description of data.** The Gene Ontology and KEGG enrichment analysis was performed on genes
852 that were significantly up- or downregulated. The number of genes associated with each significantly
853 enriched (*i.e.*, showing a Benjamini-Hochberg-adjusted *P*-value or FDR < 0.05) GO term or KEGG
854 pathway is displayed for both child (left) and adult (right) conditions. The three GO term categories
855 named 'Biological process', 'Cellular component' and 'Molecular function' are represented by blue,
856 green or orange bars, respectively. The KEGG Metabolic pathways are represented by grey bars.

857 **ADDITIONAL FILE 7**

858 **File format.** Excel spreadsheet (.xls)

859 **Title of data.** RNA-Seq Ileal Child vs Stomach Child.

860 **Description of data.** Differentially expressed genes determined by RNA-sequencing between samples
861 collected in ileal effluents of child and gastric effluents of child, and results from enrichment analyses
862 performed on significantly upregulated or downregulated genes.

863 **ADDITIONAL FILE 8**

864 **File format.** Excel spreadsheet (.xls)

865 **Title of data.** RNA-Seq Ileal Adult vs Stomach Adult.

866 **Description of data.** Differentially expressed genes determined by RNA-sequencing between samples
867 collected in ileal effluents of adult and gastric effluents of adult, and results from enrichment analyses
868 performed on significantly upregulated or downregulated genes.

869 **ADDITIONAL FILE 9**

870 **File format.** Excel spreadsheet (.xls)

871 **Title of data.** RNA-Seq Ileal Child vs Inoculum.

872 **Description of data.** Differentially expressed genes determined by RNA-sequencing between samples
873 collected in ileal effluents of child and inoculum, and results from enrichment analyses performed on
874 significantly upregulated or downregulated genes.

875 **ADDITIONAL FILE 10**

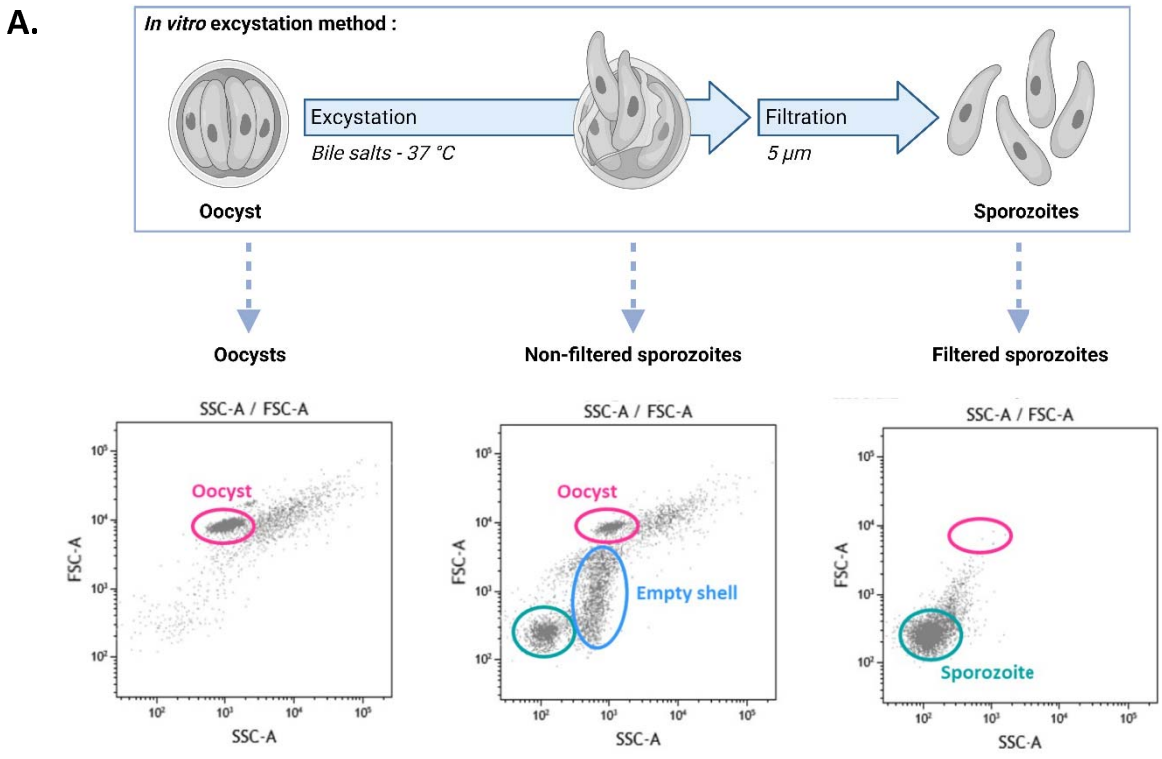
876 **File format.** Excel spreadsheet (.xls)

877 **Title of data.** RNA-Seq Ileal Adult *vs* Inoculum.

878 **Description of data.** Differentially expressed genes determined by RNA-sequencing between samples
879 collected in ileal effluents of adult and inoculum, and results from enrichment analyses performed on
880 significantly upregulated or downregulated genes.

881

Figure 2



B.

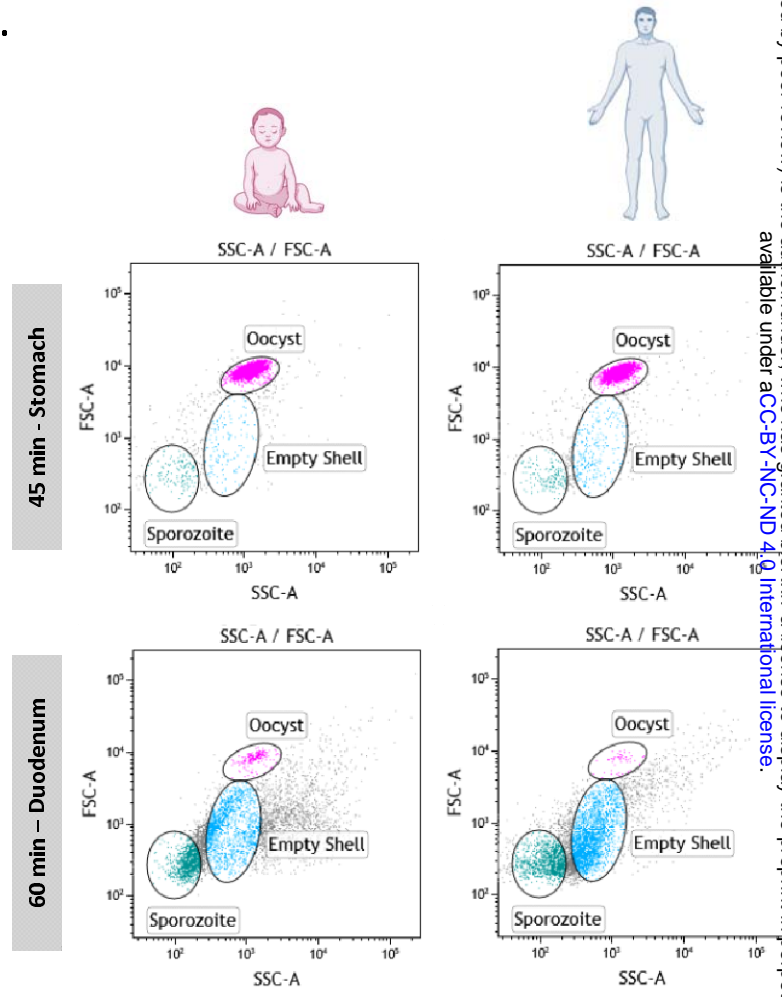
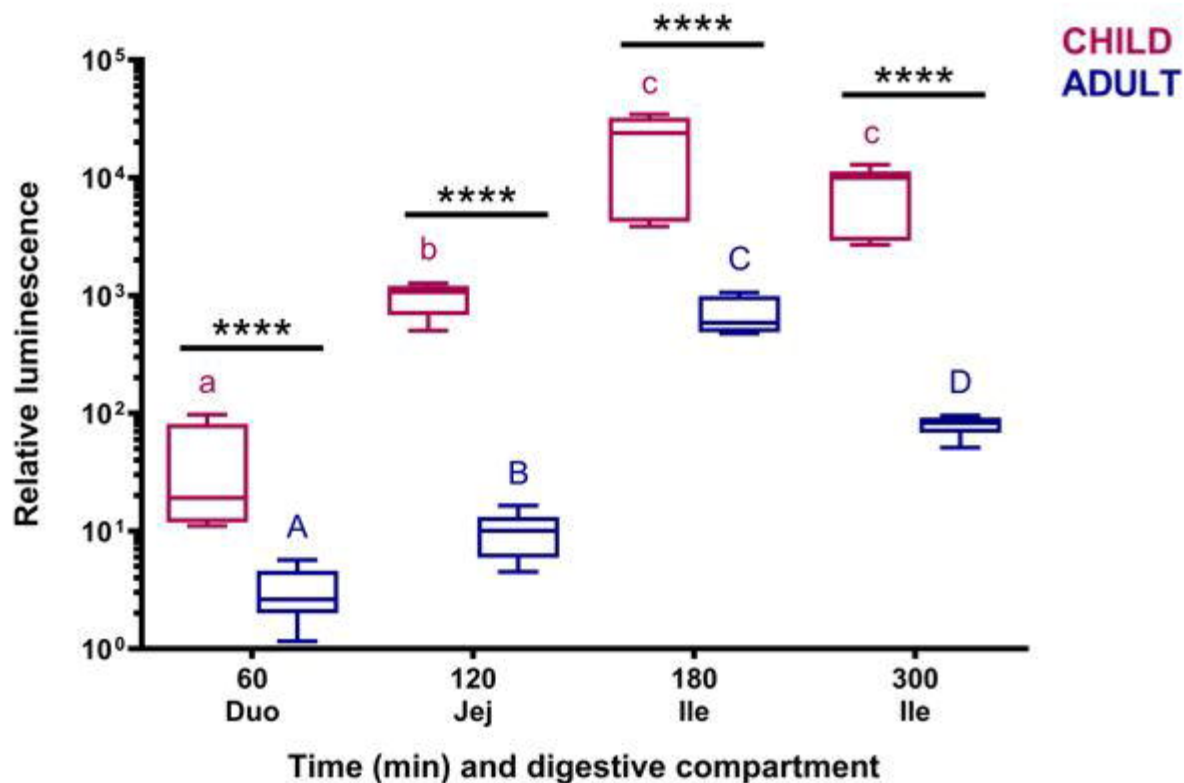


Figure 3

A.



B.

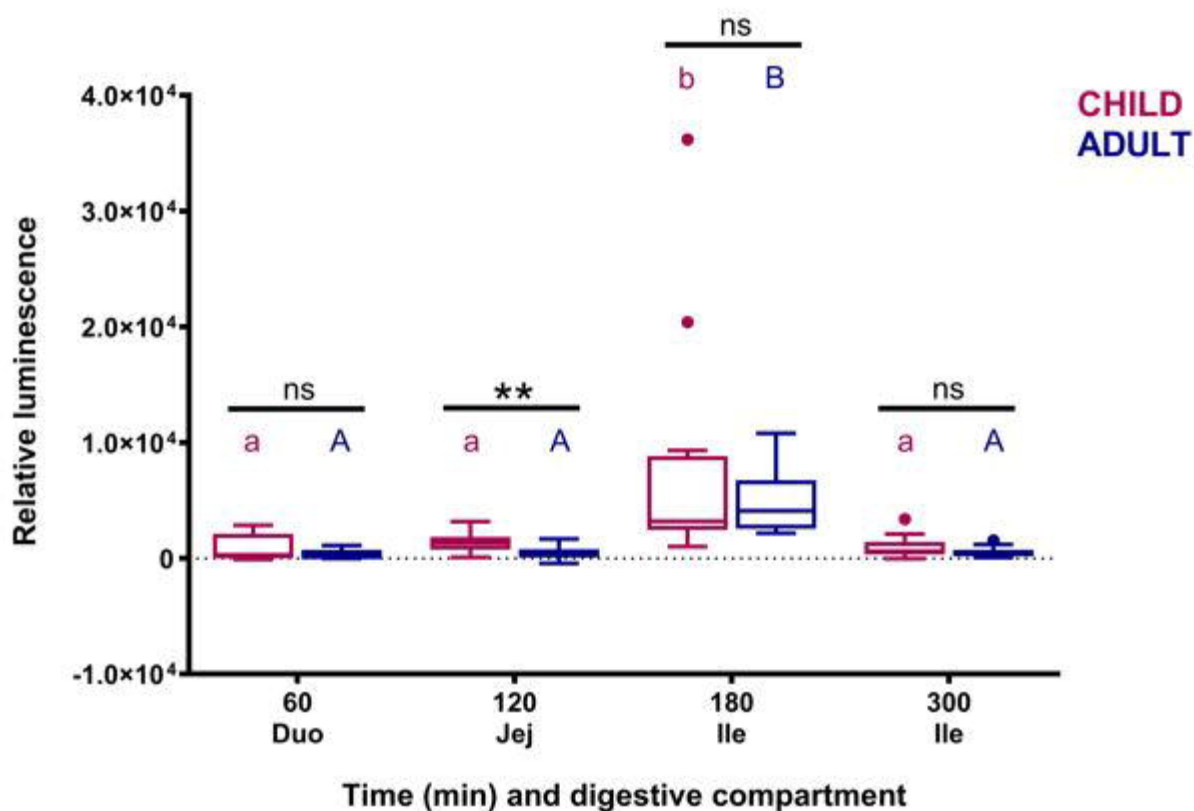
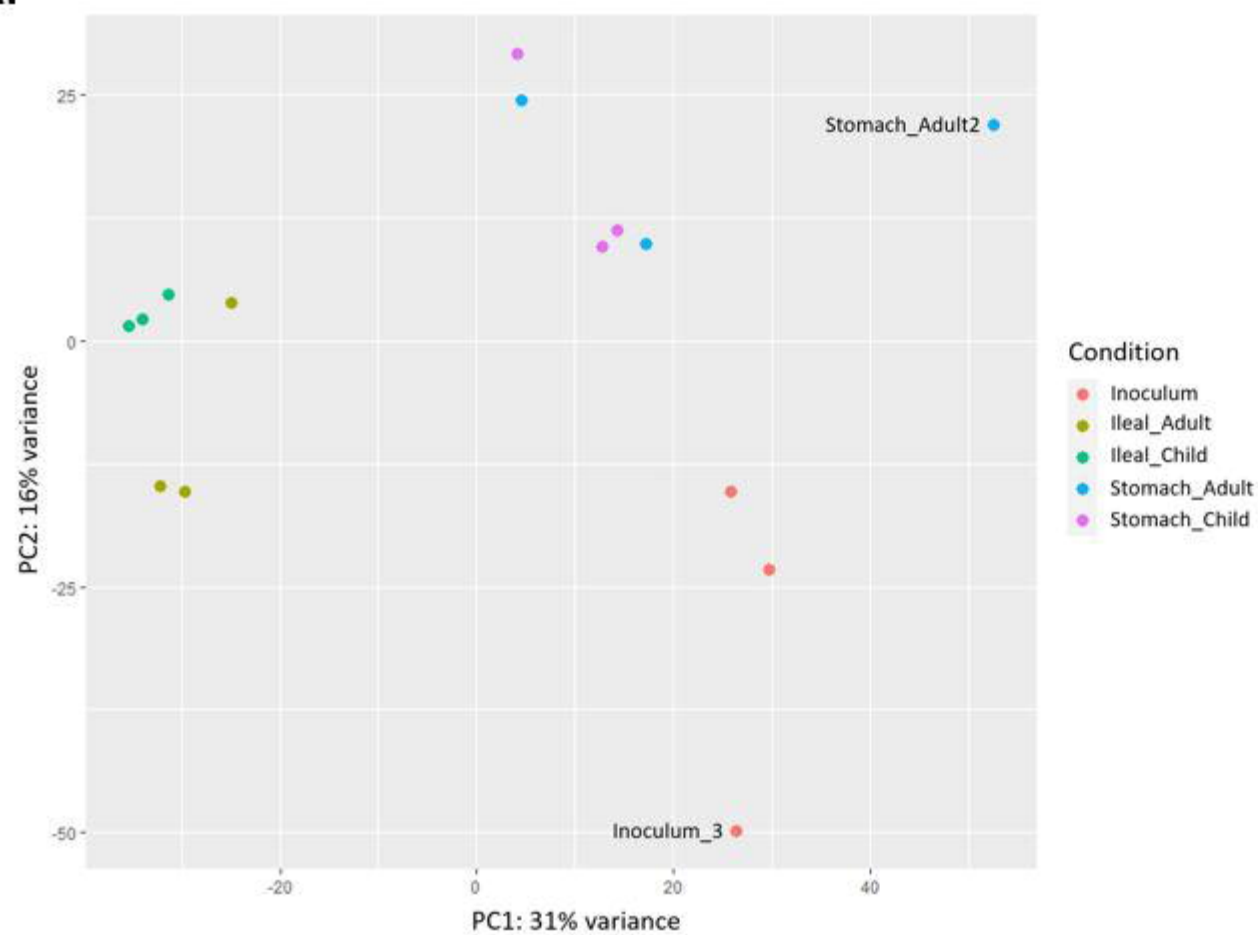
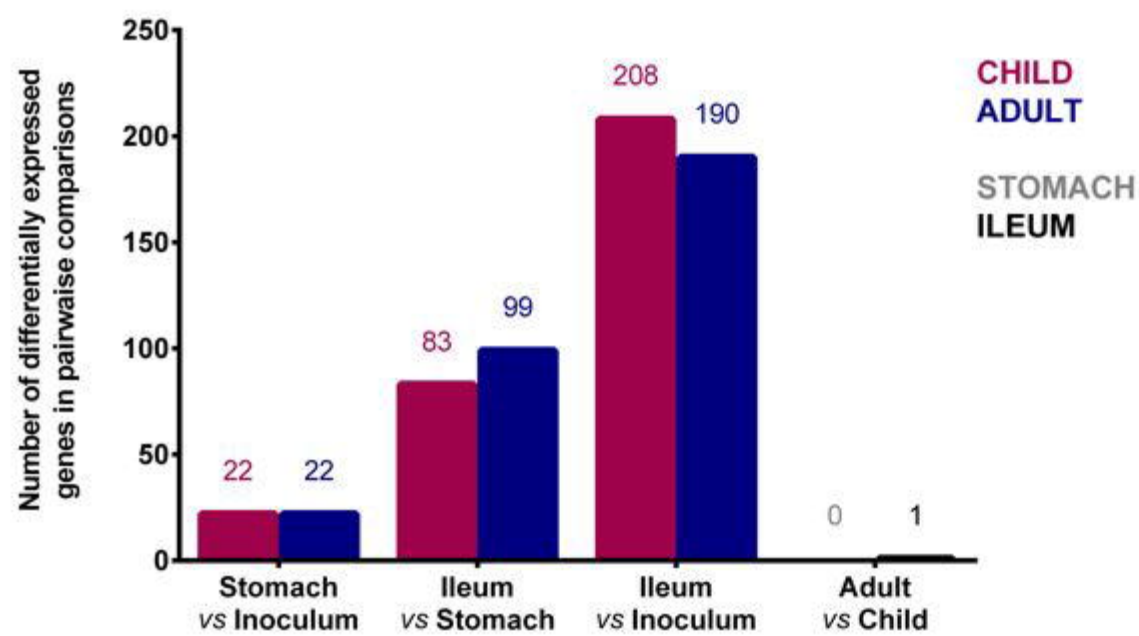


Figure 4

A.



B.



C.

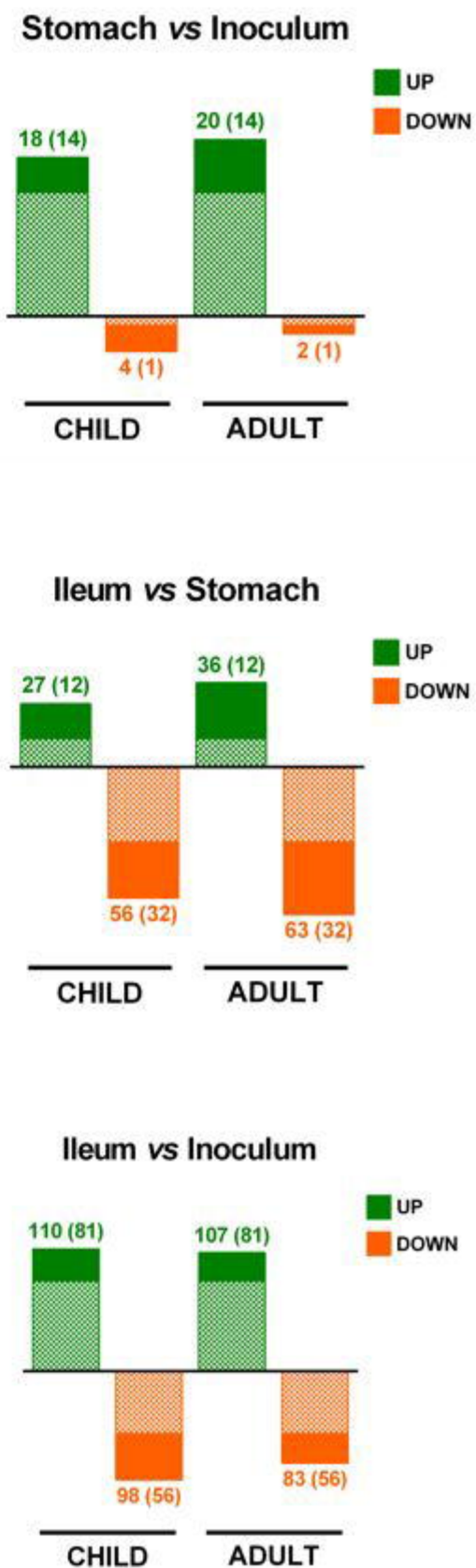
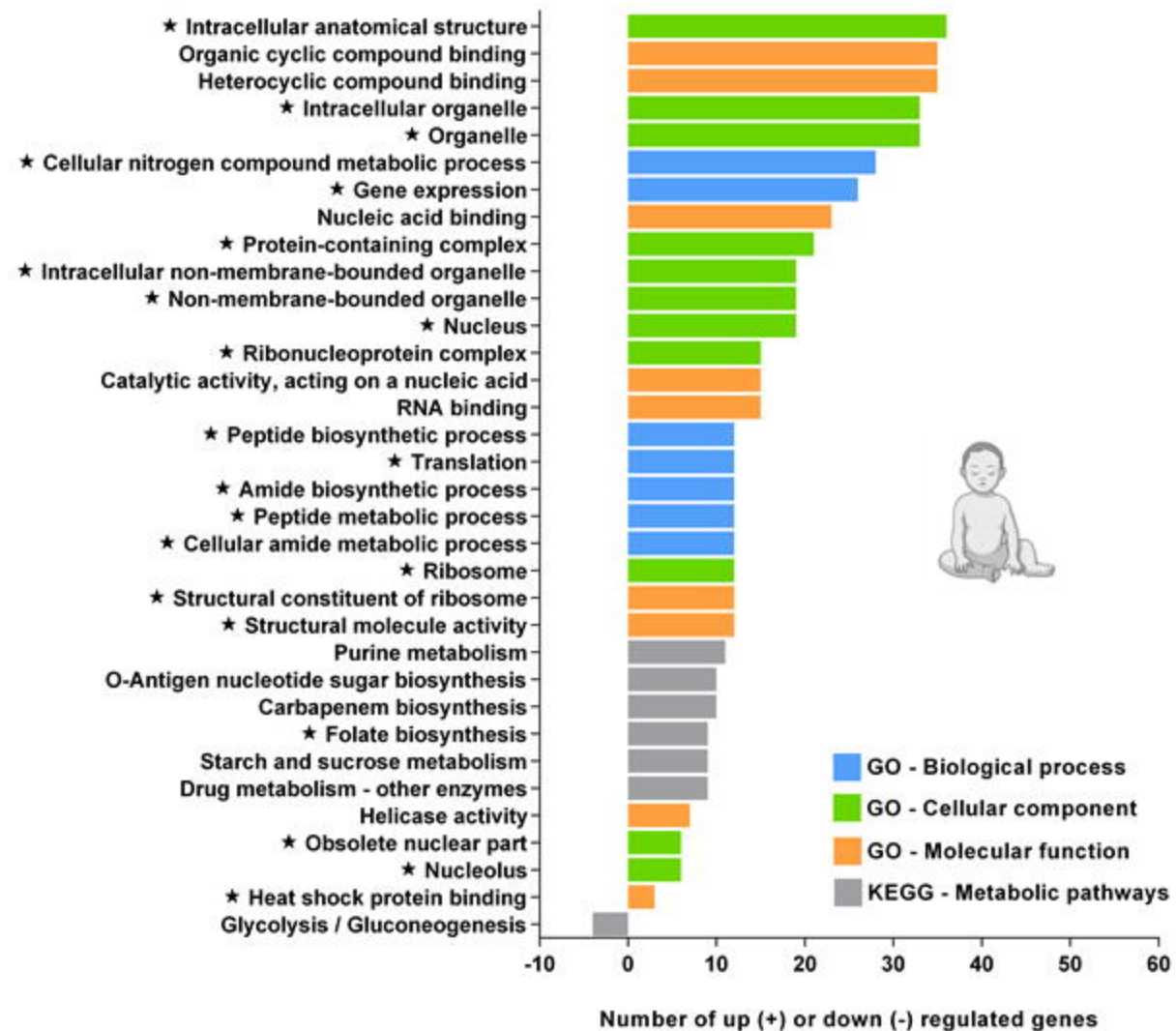


Figure 5

A.



B.

